Elevated Ubiquitin Phosphorylation by PINK1 Contributes to Proteasomal Impairment and Promotes Neurodegeneration

Cong Chen[1,#], Tong-Yao Gao[1,#], Hua-Wei Yi[4], Yi Zhang[3], Tong Wang[1], Zhi-Lin Lou[1], Tao-Feng Wei[1], Yun-Bi Lu[1], Ting-Ting Li[3], Chun Tang[2,*], Wei-Ping Zhang[1,5,*]

[1] Department of Pharmacology, Zhejiang University School of Medicine, Hangzhou 310058, China

[2] Beijing National Laboratory for Molecular Sciences, College of Chemistry and Molecular Engineering, Center for Quantitate Biology, Center for Life Science, Academy for Advanced Interdisciplinary Studies, Peking University, Beijing 100871, China

[3] Department of Biomedical Informatics, School of Basic Medical Sciences, Peking University Health Science Center, Beijing 100191, China

[4] The First People's Hospital of Jingzhou, First Affiliated Hospital of Yangtze University, Jingzhou 121001, China

[5] Zhejiang Province Key Laboratory of Mental Disorder's Management, Zhejiang University School of Medicine, Hangzhou 310058, China

[#] Equally contributed

*Corresponding authors

Chun Tang, Tang_Chun@pku.edu.cn, 292 Chengfu Road, Haidian District, Beijing 100871, China, 011-86-010-62751710

Wei-Ping Zhang, weiping601@zju.edu.cn, 866 Yuhangtang Rd, Xihu District, Hangzhou 310058, China, 011-86-0571-88208223

Abstract

Ubiquitin (Ub), a key player of protein turnover, can be phosphorylated by PINK1 kinase to generate S65-phosphorylated ubiquitin (pUb). Elevated pUb levels have been observed in aged human brains and human brains with Parkinson's disease. However, how pUb is involved in neurodegeneration remains elusive. Here we show that elevation of pUb is pervasive in a multitude of neurodegenerative conditions, including Alzheimer's disease, aging, and ischemic injury. In cultured cells, proteasomal inhibition by MG132 leads to sPINK1 accumulation, the cytosolic fragment of PINK1, thus promoting Ub phosphorylation. Elevated pUb impairs proteasomal degradation by disrupting covalent ubiquitin chain elongation and noncovalent proteasome-substrate interaction. Conversely, *pink1* knockout mitigates protein aggregation in both aging and ischemic mouse brains, as well as cells treated with MG132. Using AAV2/9 vector to specifically express sPINK1 in mouse hippocampus neurons, we observed cumulative pUb elevation, accompanied by protein aggregation, proteostasis disturbance, neuronal injury, neuroinflammation, and cognitive impairment. These sPINK1-induced impairments were reversed by co-expressing Ub/S65A phospho-null Ub mutant but exacerbated by Ub/S65E phospho-mimic mutant. As such, pUb elevation can result from declined proteasomal activity in neurodegenerative conditions, while a constant elevation of pUb actively drives neurodegeneration by further inhibiting proteasomal degradation. Our study reveals a new pathogenic pathway of neurodegeneration, highlighting the pUb-mediated feedforward loop as a promising therapeutic target for pharmaceutical intervention.

Introduction

Neurodegeneration, the hallmark of aging and neurodegenerative diseases, is characterized by irreversible loss of neurons, eventually leading to cognitive and motor impairments [1]. Neurodegeneration is often accompanied by the accumulation of ubiquitinated, potentially neurotoxic proteins, which results from impaired protein degradation machinery, particularly the ubiquitin-proteasome system (UPS) [2-4]. Essential for maintaining cellular proteostasis, the UPS not only eliminates misfolded and toxic proteins but also dynamically regulates neuronal structure and function through controlled protein turnover [5-7]. Substrate proteins are first covalently attached with K48-linked polyubiquitin chains, and the ubiquitin chains non-covalently interact with the ubiquitin-receptors in the proteasome thus targeting the substrate protein for UPS degradation [8-10]. The UPS activity can be compromised through a variety of mechanisms associated with neurodegeneration, such as modification and disassembly of the proteasome, reduced ATP level, direct inhibition by amyloid fibrils, as well as oxidative stress [1-3, 11, 12]. While these factors have been extensively investigated with the goal to identify strategies preventing the decline of proteasomal activity, the dynamic changes of ubiquitin, a central player in the UPS, have been largely overlooked in the context of neurodegeneration.

Ubiquitin itself undergoes a multitude of post-translational modifications that can alter its structure and function [13]. One such modification is phosphorylation at residue S65, installed by the kinase PINK1 (PTEN-induced putative kinase 1) [14]. An elevated level of S65-phosphorylated ubiquitin (pUb) has been observed in aged human brain and human brain with Parkinson's disease [15-17]. Additionally, two forms of PINK1 exist in cells, including the full-length PINK1 localized to the mitochondrial membrane [18, 19], and sPINK1, a

74 cytosolic fragment cleaved from PINK1 [20, 21]. Full-length PINK1 is activated upon
75 mitochondrial damage, leading to the phosphorylation of ubiquitin and Parkin, thereby
76 initiating mitophagy, a neuroprotective process for the selective removal of damaged
77 mitochondria [1, 14, 18, 22]. However, recent studies have indicated that severe and
78 persistent mitochondrial stress can paradoxically cause a failure to induce mitophagy and at
79 the same time, a sustained elevation of pUb levels [23]. Given the prevalence of
80 mitochondrial dysfunction in neurodegenerative diseases [1], pUb accumulation may result
81 from the activation of full-length PINK1 with impaired mitophagy.

82 Alternatively, elevated pUb levels may arise from inhibited proteasomal degradation.
83 The sPINK1, processed from the full-length PINK1 by mitochondria-residing proteases, is
84 normally rapidly degraded by the proteasome *per* N-end rule [20, 21]. As the UPS function is
85 often impaired under neurodegenerative conditions [1], sPINK1 may accumulate and
86 potentially phosphorylate ubiquitin, contributing to the elevation of pUb level.

87 While pUb elevation has been proposed as a potential biomarker of neurodegenerative
88 diseases [15, 16], its functional role remains poorly defined. *In vitro* studies suggest that
89 phosphorylation alters ubiquitin's structural dynamics and potentially its function [25-27].
90 Moreover, PINK1 phosphorylation inhibits ubiquitin chain elongation [28]. Since PINK1 can
91 phosphorylate both monomeric ubiquitin and covalently linked polyubiquitin [30], pUb may
92 also disrupt the noncovalent interaction between polyubiquitin conjugated to the substrate
93 protein and the proteasome. In addition, it has also been reported that Ub/S65E, a
94 phosphomimic mutant, inhibits protein turnover and reduces the cell viability of yeast when
95 exposed to stresses, including oxidative stress and unfolded protein responses [29]. Thus,
96 pUb may not simply be a biomarker but actively contribute to the neurodegenerative process.

97 Here we provide compelling evidences that pUb elevation is a driving force in
98 neurodegeneration. We demonstrate that pUb levels increase in various neurodegenerative
99 contexts, including Alzheimer's disease (AD), aging, and ischemic injury, resulting from the
100 accumulation of sPINK1 under the conditions with proteasomal impairment. Importantly, we
101 reveal that elevated pUb further inhibits proteasomal activity, forming a self-amplifying cycle
102 that perpetuates protein aggregation and neuronal damage. By dissecting this mechanism
103 from the molecular level to animal model, we uncover a general pathogenic mechanism that
104 operates across a wide spectrum of neurodegenerative disorders.

105 **Results**

106 **Elevated pUb levels are a pervasive feature of neurodegeneration**

107 Elevated pUb levels have been observed in the brains of individuals with Parkinson's
108 disease (PD) [15-17]. In the current study, we extend this observation to Alzheimer's disease
109 (AD), the most prevalent neurodegenerative dementia. We found a marked elevation of both
110 PINK1 and pUb in brain samples from AD patients compared to age- and sex-matched
111 controls (Figure 1A, B; Figure 1—table supplementary 1). This finding was further
112 corroborated in the APP/PS1 mouse model of AD, where increased PINK1 and pUb levels
113 were also detected (Figure 1C, D).

114 Beyond specific neurodegenerative diseases, pUb elevation also appears to be
115 associated with the aging process itself [15, 16], a physiological condition often accompanied
116 by gradual neurodegeneration. Here we observed a significant increase in neuronal pUb
117 levels in aged wild-type mouse brains compared to young brains (Figure 1E, F). On the other
118 hand, pUb levels in *pink1*-knockout mice remained unchanged with age and were notably
119 lower than in aged wild-type mice (Figure 1E, F).

120 We further showed that acute neurodegenerative conditions, such as cerebral ischemia,
121 also exhibit elevated pUb levels. In a mouse middle cerebral artery occlusion (MCAO)
122 model, we observed a marked increase in both PINK1 and pUb levels within the ischemic
123 core (Figure 1G, figure 1—figure supplementary 1). To further explore the relationship
124 between pUb and ischemic stress, we subjected HEK293 cells to oxygen-glucose deprivation
125 (OGD), a model mimicking ischemic conditions. Following OGD and reperfusion, we noted
126 a progressive increase in PINK1, sPINK1, and pUb levels, accompanied by a rise in protein
127 aggregation (Figure 1H, I).

128 Taken together, these findings demonstrate that pUb elevation is a common feature
129 across a wide spectrum of neurodegenerative conditions, both chronic and acute. While this
130 reinforces pUb's potential role as a biomarker, the diverse functions of ubiquitin suggest that
131 elevated pUb levels may actively contribute to the pathogenesis of neurodegeneration.

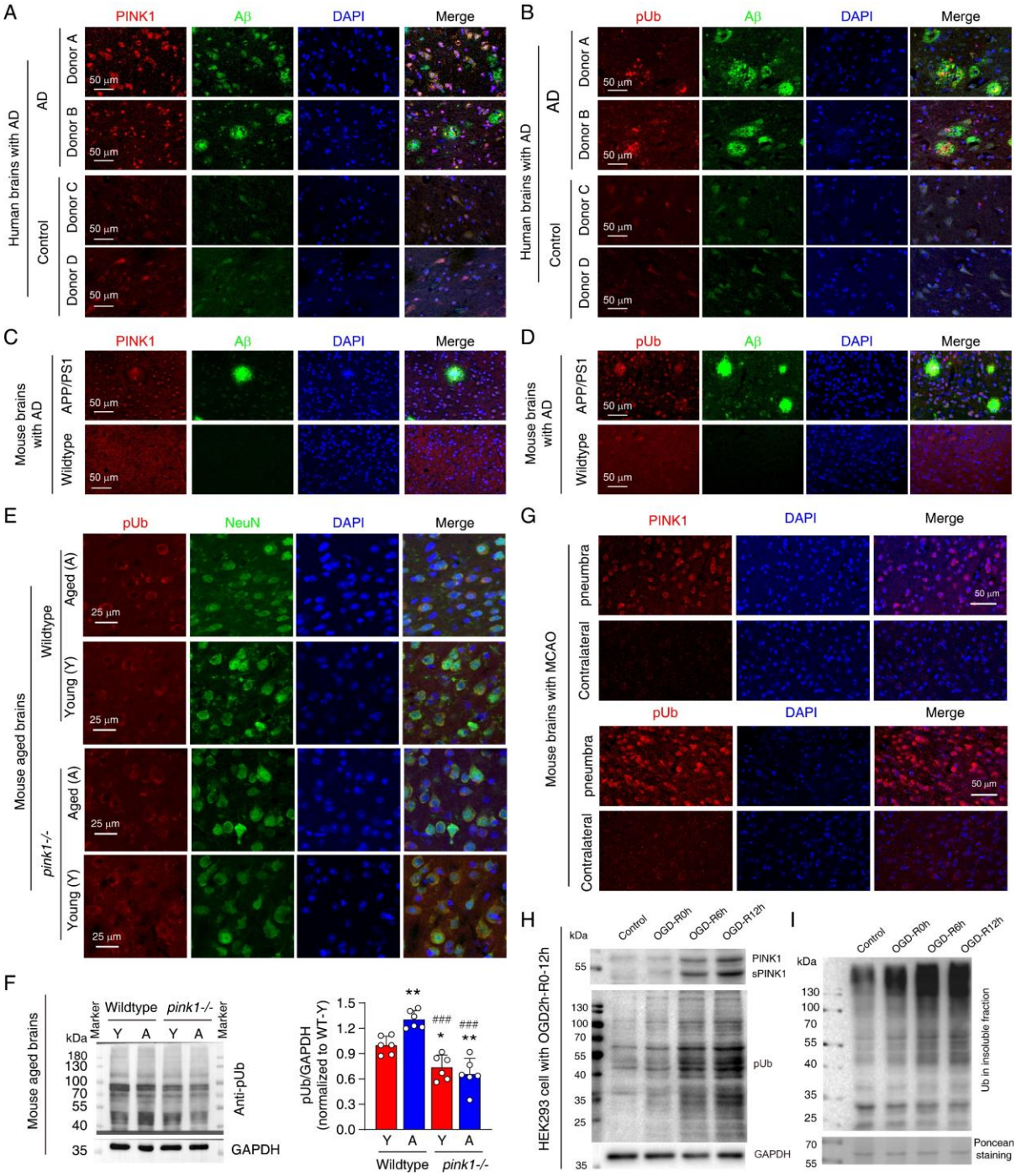

Figure 1. Elevated pUb levels in neurodegenerative conditions.

(A, B) Double immunofluorescence staining showing the distribution of PINK1 and Aβ in (A), and pUb and Aβ in (B), within the brains of AD patients compared to age-matched controls. Detailed donor demographics are available in Supplementary Table 1.

(C, D) Double immunofluorescence staining of PINK1 and Aβ (C), and pUb and Aβ (D) in the brains of wildtype and APP/PS1 transgenic mice.

(E) Double immunofluorescence staining for pUb and the neuronal marker NeuN in young and aged brains of both wildtype and *pink1-/-* mice.

(F) Western blot analysis of pUb levels in young (Y) and aged (A) wildtype and *pink1-/-* mouse brains, quantitatively comparing protein levels across ages and genotypes. $^{*}P<0.05$, $^{**}P<0.01$ for comparisons with young wildtype mice; $^{\#\#\#}P<0.001$ for comparisons with aged wildtype mice, one-way ANOVA.

(G) Immunofluorescence staining for PINK1 and pUb in the contralateral and penumbra of mouse brains subjected to MCAO for 2 hours followed by 24 hours of reperfusion. Locations of the analyzed regions are indicated in Figure S1.

(H) Western blot analysis of PINK1 and pUb levels in HEK293 cells subjected to OGD for 2 hours, followed by reperfusion at 0, 6, and 12 hours, to study changes over time.

(I) Western blot analysis of ubiquitin in the insoluble fraction of HEK293 cells post 2-hour OGD and subsequent 0, 6, 12 hours of reperfusion.

Ubiquitin phosphorylation by sPINK1 impairs proteasomal function in HEK293 cells

The activation of the full-length PINK1 is triggered by mitochondrial damage, thereby initiating mitophagy [31]. In contrast, sPINK1 is typically degraded rapidly [22], with its accumulation inversely correlating with proteasomal activity. Indeed, we observed that mitochondrial injury by using CCCP and O/A treatment primarily elevate full-length PINK1, while MG132 predominantly increases sPINK1 in HEK293 cells (Figure 2A). Further experiments showed that MG132 causes a concentration- and time-dependent increase in sPINK1 and pUb levels, with sPINK1 levels reaching a plateau after 6 hours (Figures 2B-E). In contrast, PINK1 and pUb levels remained low in *pink1*-knockout HEK293 cells treated with MG132 (Figures 2B-E), paralleling observations from organismal studies (Figure 1).

Although PINK1 activation usually involves dimerization at the mitochondrial outer membrane [19, 31], we investigated whether sPINK1 can also phosphorylate ubiquitin in the cytoplasm. We transiently transfected HEK293 cells with various PINK1 constructs: full-length PINK1, a stable cytoplasmic variant of sPINK1 (sPINK1*, PINK1/F101M/L102-L581), a kinase-dead version of this variant (sPINK1*-KD, with K219A/D362A/D384A mutations introduced) [32], and Ub^{GG}-sPINK1, a short-lived version of native sPINK1 with a ubiquitin appended at the N-terminus [20]. Western blot analysis confirmed the expression of

170 PINK1 and sPINK1* post-transfection, but not of Ub^{GG}-sPINK1 (Figure 2F). Western blot
171 analysis also showed that transfection with both PINK1 and sPINK1* increased pUb levels,
172 with sPINK1* inducing a greater increase than the full-length protein. However, transfection
173 with sPINK1*-KD or Ub^{GG}-sPINK1 did not increase pUb levels notably (Figure 2F).

174 To determine whether the elevation of pUb perturbs protein degradation while
175 minimizing its effect on mitochondria, we transiently transfect the various sPINK1 constructs
176 to increase pUb levels. Immunofluorescence showed diffuse cytoplasmic ubiquitin staining in
177 untransfected or eGFP-transfected control cells, whereas ubiquitin-positive puncta were
178 evident following MG132 treatment or in sPINK1*-transfected cells (Figure 2G). Ubiquitin-
179 positive puncta were weakly visible in Ub^{GG}-sPINK1-transfected cells (Figure 2G, 5th row,
180 indicated with arrows) but absent in sPINK1*-KD-transfected cells. Western blot analysis
181 further confirmed that MG132 treatment and sPINK1* transfection increased ubiquitin levels
182 in the insoluble fraction, while the lack of strong signal with Ub^{GG}-sPINK1 transfection
183 indicates a dose-dependent effect of PINK1 activity (Figure 2H).

184 The activation of PINK1 can also influence autophagy, and ubiquitination is a key step
185 for both autophagic and proteasomal degradation. Thus, the elevation of pUb may increase
186 protein aggregation via the inhibition of both autophagic and UPS degradation. To assess the
187 relative contribution of these two pathways on pUb-promoted protein aggregation, we treated
188 the cells with puromycin to increase ubiquitinated protein level (Figure 2I, with schematic
189 shown in the left panel). The increase of ubiquitin signal could be markedly reduced by
190 sPINK1* overexpression in comparison to neighboring cells (Figure 2I). Blocking the
191 autophagic degradation using BALA, on the other hand, we found that sPINK1*-
192 overexpression increased ubiquitin signal in comparison to neighboring cells (Figure 2I).
193 Thus, sPINK1* enhances autophagic degradation of ubiquitinated proteins, possibly via p62

phosphorylation by PINK1 as previously reported [24], while at the same time, inhibited proteasomal degradation.

To further confirm the inhibitory effect of pUb in proteasomal degradation, we assessed proteasomal activity in cells transfected with Ub-R-GFP, a model substrate for the assessment of cellular proteasomal activity [33, 34]. GFP was rapidly degraded by functional proteasomes but accumulated upon the administration of MG132. On the other hand, transfection with sPINK1* also caused GFP accumulation, while sPINK1*-KD had no effect (Figure 2J). This confirms that sPINK1* transfection lead to increased pUb levels, which impairs proteasomal degradation, mirroring the effect of MG132.

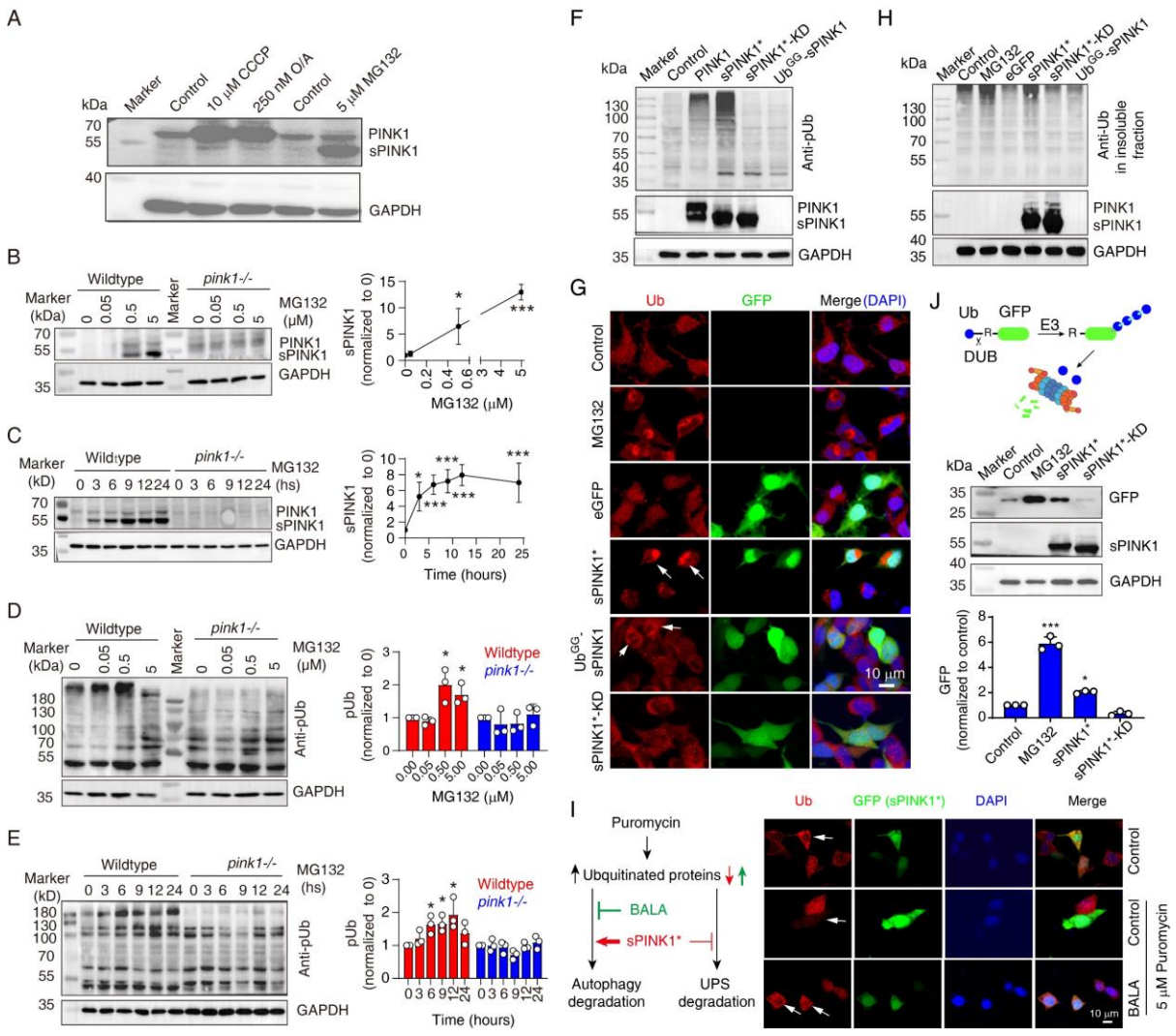

Figure 2. Impact of sPINK1-mediated Ub phosphorylation on proteasomal activity in HEK293 cells.

(A) Representative Western blot showing levels of PINK1 following the administration with CCCP, O/A, and MG132.

(B) Western blot analysis detailing the concentration-dependent effects of MG132 (0-5 μM) over 8 hours on PINK1 levels. N=3; *P < 0.05, ***P < 0.001, compared to 0 μM MG132, one-way ANOVA.

(C) Western blot analysis showing the time-dependent effects of 5 μM MG132 on PINK1 levels over 0-24 hours. N=4; *P < 0.05, ***P < 0.001, compared to 0 hours, one-way ANOVA.

(D) Western blot analysis of pUb levels under a concentration gradient of MG132 (0-5 μM) for 8 hours. N=3; *P < 0.05, compared to 0 μM MG132, one-way ANOVA.

(E) Western blot analysis of pUb levels over a time course of 24 hours with 5 μM MG132 treatment. N=3; *P < 0.05, compared to 0 hours, one-way ANOVA.

(F) Western blot analysis showing levels of pUb and PINK1 following transfection with various PINK1 constructs: sPINK1* (PINK1/F101M/L102-L581), sPINK1*-KD (kinase-dead sPINK1* with additional K219A/D362A/D384A mutations), and Ub^{GG}-sPINK1 (a short-lived version of native sPINK1 with an appended N-terminal Ub).

(G) Representative immunofluorescence images of Ub staining in cells treated with MG132 or transfected with various sPINK1 constructs, highlighting differences in ubiquitin localization and aggregation. The white arrows indicate positively transfected cells.

(H) Western blot analysis of Ub in the insoluble fraction of cell lysates following treatment with 5 μM MG132 or after transfection with different sPINK1 constructs.

(I) Immunofluorescence staining of Ub differentiating the roles of sPINK1 over-expression on proteasomal and autophagic degradation of puromycin increased unfolded proteins. The left panel illustrates the experimental strategy. Puromycin (5 μg/ml) was applied 2 hours before harvesting with or without 0.1 μM BALA (an autophagy inhibitor). The white arrows indicate positively transfected cells.

(J) Western blot analysis showing GFP degradation in HEK293 cells, with the top panel illustrating the Ub-GFP construct, a model substrate to evaluate proteasomal degradation efficiency. N=3; *P < 0.05, ***P < 0.001, compared to the control group, one-way ANOVA.

pUb impairs proteasomal activity via covalent and noncovalent mechanisms

To understand how ubiquitin phosphorylation affects UPS degradation, we first assessed ubiquitin chain formation *in vitro*. While unmodified ubiquitin efficiently formed di-, tri-, and higher-order chains with E1 and E2 enzymes, pUb predominantly produced di-Ub chains (Figure 3A), consistent with the previous report [28]. The introduction of S65A

239 (phospho-null) and S65E (phospho-mimetic) mutations into ubiquitin provided further
240 insights into the effects of phosphorylation. The Ub/S65A mutation facilitated chain
241 elongation similar to the unmodified Ub, whereas Ub/S65E mutation largely resulted in di-
242 Ub formation but not higher-order chains (Figure 3A). Although the Ub/S65E mutant may
243 not completely mimic all characteristics of pUb, it effectively demonstrates the impact of S65
244 phosphorylation on chain formation.

245 We also investigated K48-linked ubiquitin chain formation in HEK293 cells expressing
246 FLAG-tagged Ub/K48-only mutant (FLAG-Ub/48K). Following proteasome inhibition with
247 MG132, K48-linked chains accumulated in wildtype and *pink1-/-* cells, but not in cells
248 overexpressing full-length PINK1 or sPINK1* (Figure 3B).

249 Since PINK1 can phosphorylate both ubiquitin monomers and polyUb chains [30], we
250 next investigated the impact of pUb chains on proteasomal degradation. *In vitro* degradation
251 assays with purified proteasomes showed that degradation of K48-linked pUb-chain-modified
252 GFP (pK48-polyUb-GFP) was slower compared to the unmodified counterpart (K48-polyUb-
253 GFP) (Figure 3C, figure 3—figure supplementary 1, 2). The interactions between
254 ubiquitinated substrates and immobilized proteasomes were then analyzed using total internal
255 reflection fluorescence (TIRF) microscopy following an established protocol [35]. The assays
256 revealed fewer Ub-GFP puncta for pK48-polyUb-GFP compared to unphosphorylated
257 controls (Figure 3D, E, figure 3—figure supplementary 3), and these puncta dissociated more
258 rapidly from the proteasomes, suggesting a shorter dwell time of the proteasome-substrate
259 complex (Figure 3F-I, figure 3—figure supplementary 4).

260 Collectively, these findings demonstrate that elevated pUb levels not only disrupt
261 covalent ubiquitin chain elongation and subsequent substrate ubiquitination, but also hinder

the non-covalent binding of ubiquitinated substrates to the proteasome. Both mechanisms significantly contribute to the impairment of proteasomal activity.

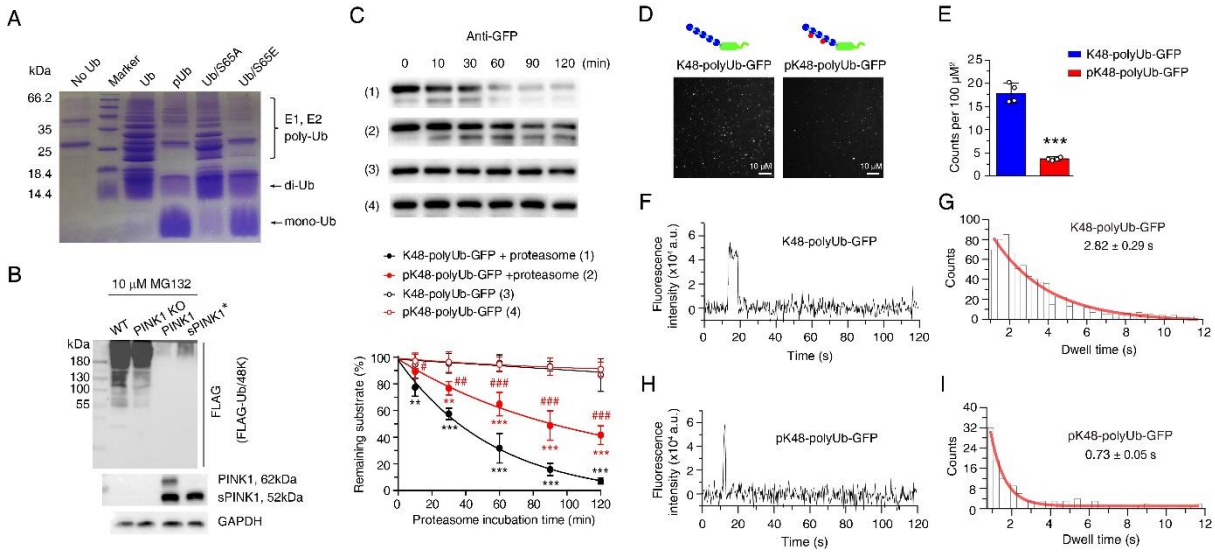

Figure 3. Impact of ubiquitin phosphorylation on chain elongation and proteasomal association.

(A) Coomassie blue staining showing Ub chain formation using different Ub variants as building blocks: wildtype Ub, phosphorylated Ub (pUb), phospho-null Ub/S65A, and phospho-mimic Ub/S65E.

(B) Analysis the transfection and knockout of PINK1 on K48-linked Ub chain formation in HEK293 cells treated with 10 μM MG132. Cells were transfected with FLAG-tagged Ub/48K. Additionally, *pink1-/-* cells were transfected with either full-length PINK1 or the sPINK1* variant.

(C) *In vitro* proteasomal degradation assay of GFP modified with K48-linked ubiquitin chains (K48-polyUb-GFP) versus with phosphorylated K48-linked ubiquitin chains (pK48-polyUb-GFP). N=3; $^{**}P<0.01$, $^{***}P<0.001$ compared to respective controls without added proteasome; $^{\#}P<0.05$, $^{\#\#}P<0.01$, $^{\#\#\#}P<0.001$ compared to K48-polyUb-GFP with proteasome, two-way ANOVA.

(D) Representative TIRF microscopy images showing the binding of K48-polyUb-GFP (left) and pK48-polyUb-GFP (right) to surface-immobilized proteasomes, visualized as bright puncta.

(E) Quantitative analysis of puncta density from TIRF images, with N=4; $^{***}P<0.001$ compared to K48-polyUb-GFP, using a paired t-test.

(F, H) Representative fluorescence traces of a single punctum for K48-polyUb-GFP (F) and pK48-polyUb-GFP (H), detailing the dynamic interactions at the proteasome surface.

(G, I) Analysis of GFP fluorescence dwell time for K48-polyUb-GFP (G) and pK48-polyUb-GFP (I). Data are binned and modeled with a single exponential decay curve (red line), illustrating differences in substrate-proteasome interaction durations.

286 ***pink1* knockout mitigates protein aggregation resulting from declined proteasomal**
287 **activity**

288 Aging and neurodegenerative diseases commonly feature accumulations of protein
289 aggregates alongside decreased proteasomal activity [36]. Our findings have shown that
290 conditions with impairing proteasomal function, such as Alzheimer's disease, cerebral
291 ischemia, aging, and pharmacologic treatment of proteasome inhibitor, result in increased
292 levels of sPINK1 and pUb. As elevated pUb could in turn inhibit the UPS degradation, we
293 hypothesized that proteasomal inhibition and pUb elevation form a positive feedback loop
294 contributing to protein aggregation, while *pink1* knockout disrupts this process (Figure 4A).

295 In support of this hypothesis, we found that aged wildtype mice exhibited distinct Ub-
296 positive puncta in neurons and increased insoluble ubiquitin levels, indicative of protein
297 aggregation. In contrast, aged *pink1-/-* mice showed no such age-related changes in ubiquitin
298 staining or insoluble ubiquitin levels (Figure 4B, C). Following MCAO, insoluble ubiquitin
299 levels were significantly elevated in the ipsilateral hemisphere of wildtype mice, but not in
300 *pink1-/-* mice (Figure 4D).

301 To directly assess the link between proteasomal inhibition, elevated pUb level, and
302 protein aggregation, we treated wildtype and *pink1-/-* cells with MG132. As expected,
303 MG132 induced an increase in insoluble ubiquitin levels in both cell types in a concentration-
304 and time-dependent manner (Figure 4E, F). However, the accumulation of ubiquitin-positive
305 aggregates occurred significantly slower in *pink1-/-* cells, even though they eventually
306 reached levels comparable to those in wildtype cells at 24 hrs after MG132 administration
307 (Figure 4F). This suggests that PINK1 deficiency delays the onset and progression of protein
308 aggregation, but does not completely prevent it. Intriguingly, MG132 treatment also
309 increased LC3-II levels, a marker of autophagy, in wildtype cells, possibly indicating either

activation of autophagy or reduced LC3 degradation as a compensatory response to proteasomal inhibition (Figure 4G, H). Conversely, LC3-II levels did not increase in *pink1-/-* cells following MG132 treatment (Figure 4G, H). This indicates that PINK1 is required for autophagy activation under proteasome stress, aligning with our observations of enhanced autophagy upon PINK1 overexpression (Figure 2I).

Together, the results indicate that *pink1* knockout can alleviate protein aggregation associated with aging, ischemic injury, or proteasomal inhibition by disrupting the self-amplifying cycle of proteasomal impairment (Figure 4A).

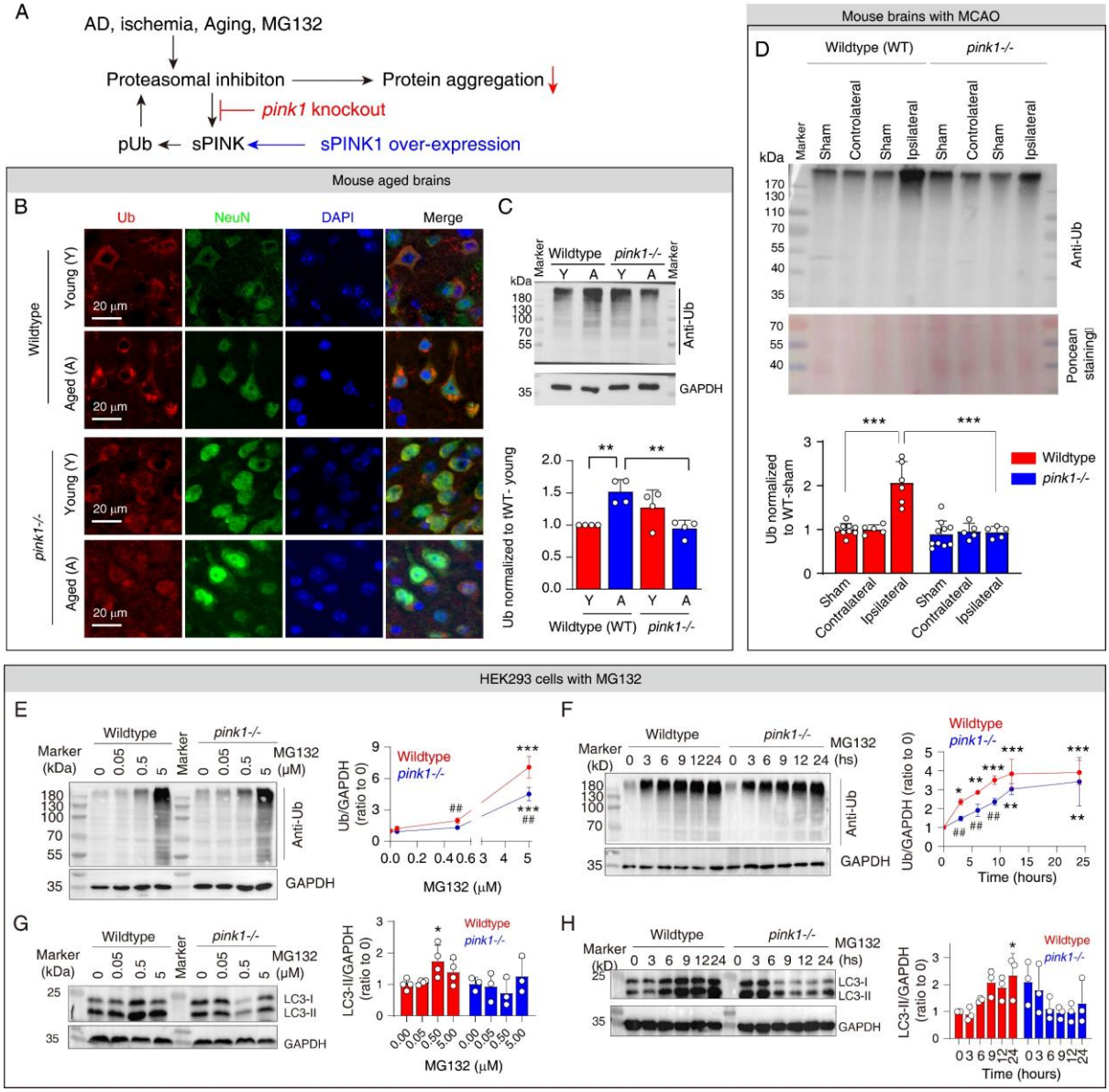

319 **Figure 4. *pink1* knockout mitigates protein aggregation under proteasomal inhibition.**

320 **(A)** Schematic representation illustrating the reciprocal feed-forward cycle among proteasomal
321 inhibition, and the elevation of sPINK1 and pUb levels.

322 **(B)** Immunofluorescence staining of Ub in the brains of young and aged wildtype and *pink1-/-* mice.

323 **(C)** Western blot analysis quantifying Ub in the insoluble protein fraction from young and aged mouse
324 brains. Statistical analysis includes N=4; **P<0.01, one-way ANOVA.

325 **(D)** Western blot analysis of Ub in the insoluble protein fraction of wildtype and *pink1-/-* mouse
326 brains subjected to MCAO for 2 hours followed by 24 hours of reperfusion. Comparison includes the
327 sham-operated group (same procedure without occlusion). Locations of the analyzed regions
328 (contralateral and ipsilateral) are indicated in Figure 1—figure supplementary 1.

329 **(E)** Western blot analysis of Ub levels in the insoluble fraction following treatment with 0-5 μM
330 MG132 for 8 hours. N=3; ***P<0.001 compared to 0 μM MG132; $^{\#\#}P$<0.01 compared with wildtype
331 cells, one-way ANOVA.

332 **(F)** Western blot analysis of Ub levels in the insoluble fraction following treatment with 5 μM MG132
333 over a 0–24-hour period. N=4; *P<0.05, **P<0.01, ***P<0.001 compared to 0 μM MG132; $^{\#\#}P$<0.01
334 compared with wildtype cells, one-way ANOVA.

335 **(G)** Western blot analysis of LC3 levels following treatment with 0-5 μM MG132 for 8 hours. N=4;
336 *P<0.05 compared to 0 μM MG132, one-way ANOVA.

337 **(H)** Western blot analysis of LC3 levels after 5 μM MG132 treatment over 0-24 hours. N=3; *P<0.05
338 compared to 0 μM MG132, one-way ANOVA.

339

340 **sPINK1* overexpression causes cumulative proteome-wide changes**

341 As illustrated in Figure 4A, the over-expression of sPINK1 may lead to a sustained
342 elevation of pUb and cause protein aggregation. Since protein aggregation is one of primary
343 causes for neurodegeneration, we assessed the impact of pUb elevation on neurons. First, we
344 confirmed the roles of sPINK1 and phosphomimetic Ub/S65E mutant on protein aggregation
345 in SH-SY5Y cell, a neuroblast-link cell line. Ubiquitin-positive puncta was observed in cells
346 treated with MG132 and overexpressing either sPINK1* or Ub/S65E (Figure 5—figure
347 supplementary 1), similar to the findings in HEK293 cell (Figure 2G).

348 It has been shown that the phospho-null mutant Ub/S65A could mitigate, while the
349 phospho-mimic Ub/S65E could mimic, the effects produced by PINK1 through the

350 phosphorylation of ubiquitin [29]. Thus, we specifically overexpressed sPINK1*, sPINK1*
351 with Ub/S65A (sPINK1*+Ub/S65A), Ub/S65E, or GFP control in mouse hippocampal
352 neurons using AAV2/9, and the specific expression was confirmed through GFP co-
353 localization with fluorescence staining of NeuN in the CA1 region (Figure 5—figure
354 supplementary 2). While no changes were observed at 10 days post-transfection, significant
355 neuronal loss was evident at 30 and 70 days in mice expressing Ub/S65E, but not in other
356 three groups (Figure 5—figure supplementary 2). Additionally, Ub/S65E induced glial
357 responses at 30- and 70-days post transfection, as demonstrated by GFAP/Iba1 staining and
358 GFAP/CD11b Western blots (Figure 5—figure supplementary 3, 4). In contrast, the sPINK1*
359 and sPINK1*+Ub/S65A groups showed an increase in GFAP (indicative of astrocyte
360 activation) at 70-days post transfection, without effects on Iba1 or CD11b (Figure 5—figure
361 supplementary 3, 4). The existence of GFAP response may be caused by potential neuronal
362 injury at 70-days post-transfection.

363 To investigate the molecular underpinnings of sPINK1*-induced neuronal injury, we
364 performed proteomic analysis of mouse hippocampus at 30- and 70-days post-transfection
365 (Figure 5—dataset supplementary 1). Despite similar number of total proteins identified
366 between the GFP and sPINK1* groups (Figure 5—figure supplementary 5A-D), notable
367 differences emerged. For example, the neuronal injury/neuroinflammation marker HMGB1
368 was elevated at both time points with sPINK1* overexpression, while the mitochondrial
369 marker Tom20 showed a decrease only at 70 days, indicating a delayed loss of mitochondria.

370 Gene set enrichment analysis (GSEA) further revealed a time-dependent impact on
371 mitochondrial function. At 30-days, changes in proteins related to mitophagy, mitochondrial
372 organization, and respiratory electron transport suggested an initial compensatory response to
373 mitochondrial stress (Figure 5—figure supplementary 5D). However, at 70-days, these

374 changes expanded to include broader mitochondrial dysfunction and apoptotic processes,
375 culminating in mitochondrial loss and neuronal injury (Figure 5—figure supplementary 5D).

376 Further GO analysis underscored the extensive proteomic dysregulation caused by
377 sPINK1* overexpression (Figure 5—figure supplementary 5F-H). At 70-days, a large number
378 of proteins were both upregulated and downregulated, indicative of disrupted proteostasis.
379 This could be attributed to proteasomal inhibition or a stress response to protein aggregates.
380 For example, we observed a significant up-regulation of RNA-binding and RNA-processing
381 proteins. Similar proteome-wide change has been noticed in the Ub/S65E over-expressed
382 yeast [29]. Importantly, we found many affected proteins were associated with the disruption
383 of synaptic functions and neuronal projections, while downregulated proteins were linked to
384 myelination, synaptic maturation, and lipid metabolism (Figure 5—figure supplementary 5F-
385 H). Note that many of these changes were insignificant at 30-days post-transfection (Figure
386 5—figure supplementary 5F-H). These findings collectively underscore the systemic impact
387 of sPINK1* overexpression on neuronal structure and function, which likely drives
388 progressive neuronal injury.

389 **Elevated pUb levels drive protein aggregation in mouse hippocampal neurons**

390 To assess the impact of elevated pUb on protein aggregation *in vivo*, we examined
391 PINK1 and pUb levels in the mouse hippocampus following sPINK1* overexpression. At 30-
392 days, a distinct band for sPINK1 was observed, accompanied by a significant increase in pUb
393 levels (Figure 5A). At 70-days, three distinct bands that could be assigned to sPINK1, full-
394 length PINK1, and ubiquitinated PINK1 (Figure 5B). The presence of full-length PINK1
395 indicates mitochondrial injury, while ubiquitinated PINK1 suggests compromised
396 proteasomal activity. Notably, co-expression of Ub/S65A yielded only a faint sPINK1 band
397 (Figure 5B), indicating its potential to counteract the proteasomal inhibition induced by

398 sPINK1*, thereby promoting degradation of this stable sPINK1 variant. Consequently, pUb
399 levels were elevated with sPINK1* overexpression but remained at control levels with
400 sPINK1* and Ub/S65A co-expression (Figure 5C).

401 Immunofluorescence staining revealed ubiquitin puncta in hippocampal neurons
402 overexpressing sPINK1*, sPINK1+Ub/S65A, or Ub/S65E (Figure 5D). Western blot analysis
403 showed an increase in soluble ubiquitin in brains from the sPINK1*+Ub/S65A group, likely
404 arising from the overexpressed Ub/S65A (Figure 5E). Levels of insoluble ubiquitin were
405 significantly elevated in the sPINK1*, sPINK1*+Ub/S65A, and Ub/S65E groups (Figure 5F).
406 Notably, proteins smaller than 70 kDa accumulated in the sPINK1* and Ub/S65E groups,
407 indicating the inhibition of ubiquitin chain elongation as observed *in vitro* (Figure 3B), but
408 not in the sPINK1*+Ub/S65A group. Furthermore, the overexpression of sPINK1*,
409 sPINK1*+Ub/S65A, or Ub/S65E had minimal impact on autophagic flux, as indicated by
410 stable LC3-II and p62 levels (Figure 5—figure supplementary 6). These findings suggest that
411 the observed protein aggregation is primarily driven by elevated pUb levels and the resulting
412 proteasomal dysfunction.

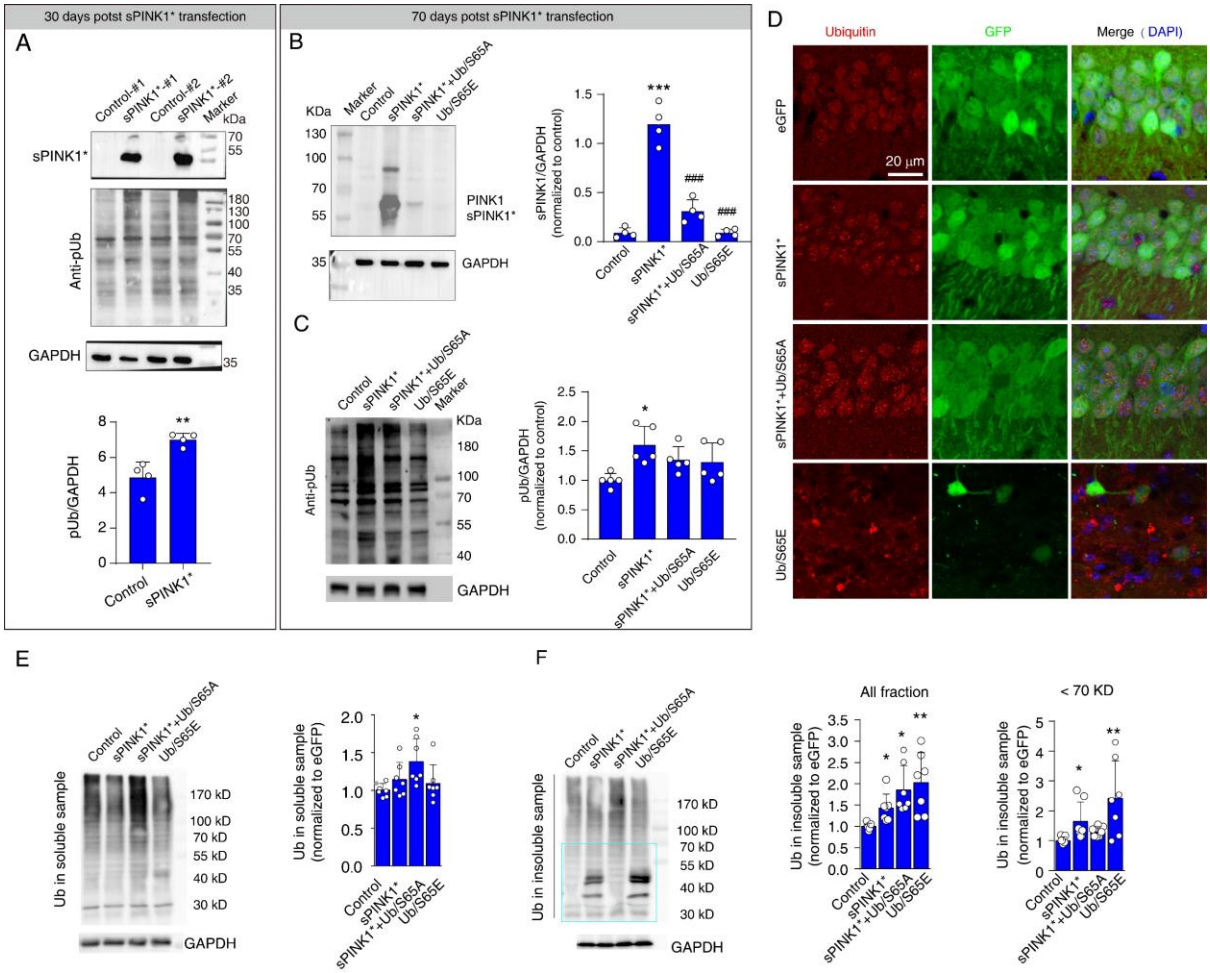

Figure 5. Elevated pUb levels induce protein aggregation in mouse hippocampal neurons.

(A) Western blot analysis showing levels of PINK1 and pUb in mouse hippocampus at 30-days post-transfection. *N*=4; ***P*<0.01 compared with control, one-way ANOVA.

(B) Western blot analysis of PINK1 in the mouse hippocampus at 70-days post-transfection, illustrating changes in expression over time. *N*=4; ***P*<0.001 compared with control; $^{\#\#\#}P$<0.001 compared with sPINK1, one-way ANOVA.

(C) Western blot analysis of pUb in the mouse hippocampus at 70-days post-transfection, highlighting the persistence of phosphorylation changes. *N*=5; **P*<0.05 compared with control, one-way ANOVA.

(D) Representative immunofluorescence images depicting ubiquitin staining in the CA1 region of the mouse hippocampus at 70-days post-transfection.

(E) Western blot analysis of ubiquitin in the soluble fraction of hippocampal lysates at 70-days post-transfection. *N*=7; **P*<0.05 compared with control, one-way ANOVA.

(F) Western blot analysis of Ub in the insoluble fraction of hippocampal lysates at 70-days post-transfection. Quantitative analysis includes total protein and specifically proteins smaller than 70 kDa. *N*=7; **P*<0.05, ***P*<0.001 compared with control, one-way ANOVA.

430 **Elevated pUb levels impair neuronal integrity and cognitive function**

431 To determine the impact of pUb-induced protein aggregates on neuronal function, we
432 conducted behavioral tests on mice at 70-days post-transfection. Overexpression of sPINK1*
433 or Ub/S65E significantly impaired cognitive functions, evidenced by reduced performance in
434 novel object recognition (Figure 6A, B) and fear conditioning tests (Figure 6C, D). Notably,
435 co-expression of Ub/S65A with sPINK1* ameliorated sPINK1*-induced cognitive deficits,
436 suggesting a protective effect against pUb-caused impairments.

437 Consistent with these behavioral findings, Western blot analysis showed decreased
438 levels of Tom20, a mitochondrial marker, in brains overexpressing sPINK1*. This
439 mitochondrial deficit was reversed when Ub/S65A was co-expressed (Figure 6E), aligning
440 with the proteomic data (Figure 5—figure supplementary 5D). Additionally, we noted
441 reduced levels of MAP2, a dendritic marker, and PSD95, a postsynaptic density marker, in
442 the brains expressing sPINK1* and Ub/S65E. These reductions were restored to normal
443 levels upon Ub/S65A co-expression (Figure 6F, G). Accordingly, Golgi staining revealed a
444 decrease in dendritic spine density following sPINK1* overexpression, which was reversed
445 upon Ub/S65A co-expression (Figure 6H). In contrast, Ub/S65E overexpression led to more
446 severe dendritic and spine loss, with notably slimmer dendrites and a significant reduction in
447 spine density compared to sPINK1* (Figure 6H).

448 These findings underscore that sPINK1*-induced neuronal damage accumulates over
449 time and can be effectively mitigated by co-expressing the phospho-null mutant Ub/S65A.
450 Conversely, the phospho-mimic Ub/S65E exacerbates neuronal damage rapidly. Collectively,
451 these results demonstrate that elevated pUb level contributes to hippocampal neuronal injury
452 and associated cognitive impairments, highlighting its significance as a driver of
453 neurodegeneration.

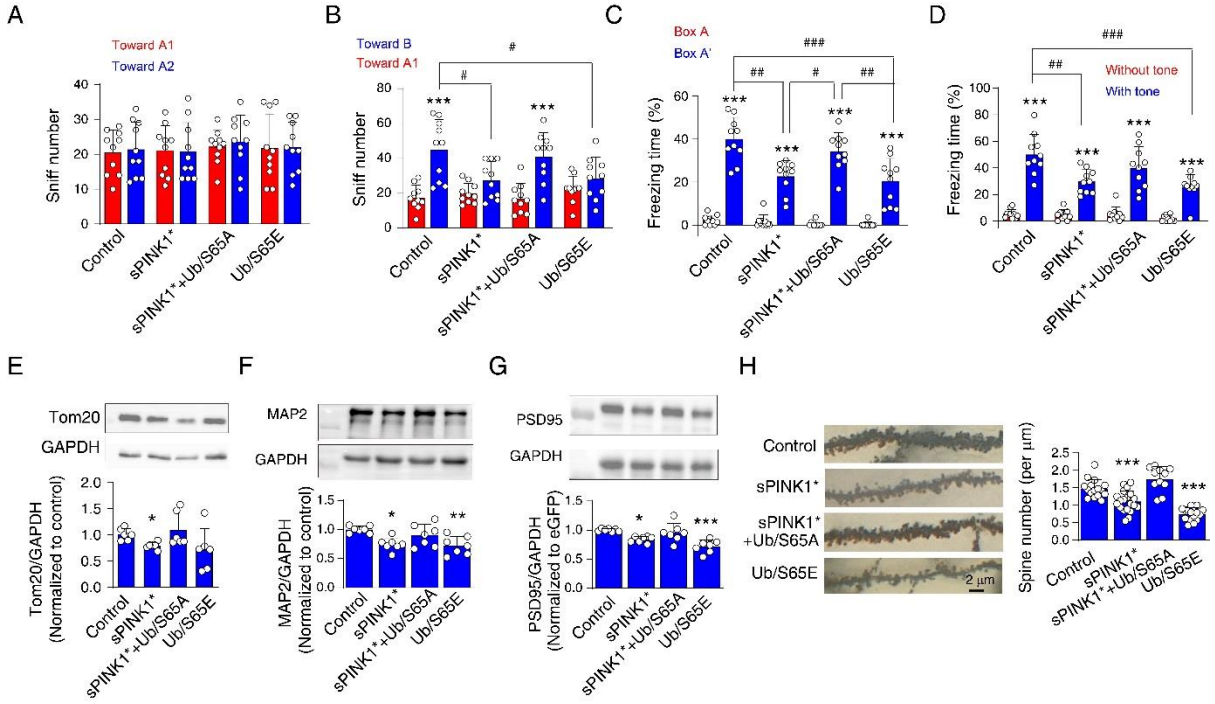

Figure 6. Elevated pUb levels induce neuronal injury in mouse brains.

(A, B) Novel object recognition test showing the sniff number to objects during training (A) and testing (B) phases. N=10; ***P<0.001 compared with the sniff number toward A1 object during training, paired t-test. $^{\#}P$<0.05, one-way ANOVA.

(C, D) Fear conditioning tests evaluating contextual (C) and cued (D) memory. N=10; ***P<0.001 compared with Box A (contextual) or absence of tone (cued), paired t-test. $^{\#}P$<0.05, $^{\#\#}P$<0.01, $^{\#\#\#}P$<0.001, one-way ANOVA.

(E-G) Western blot analysis measuring levels of mitochondrial, dendritic, and synaptic markers: Tom20 (E), MAP2 (F), and PSD95 (G) in the mouse hippocampus. N=7; *P<0.05, **P<0.01, ***P<0.001 compared with control, one-way ANOVA.

(H) Golgi staining used to assess hippocampal neuronal spines and dendrites. The left panel shows representative images; the right panel provides a statistical analysis of spine density on hippocampal neuron dendrites from 3 mice. ***P<0.001 compared with control, one-way ANOVA.

Discussion

In the current study, we demonstrate that elevated pUb level is a pervasive feature in both chronic and acute neurodegenerative conditions. This observation aligns with previous reports of sustained pUb elevation in human brains with PD [15, 16]. Our findings extend this

473 phenomenon to AD, aging, and cerebral ischemia. While severe mitochondrial injury has
474 been implicated as a mechanism leading to pUb elevation [23, 37], we have uncovered an
475 additional contributing factor. We show that inhibition of proteasomal degradation stabilizes
476 sPINK1 in the cytoplasm, where it retains its ability to phosphorylate ubiquitin.

477 Proteasomal inhibition can be caused by various pathological factors in
478 neurodegeneration [1]. Cerebral ischemia, for instance, induces ATP deficiency, while
479 hypoxia and the secondary effect of oxidative stress would further lead to proteasomal
480 modification and impairment of proteasomal function [11, 38]. On the other hand, in AD,
481 amyloid fibrils can directly block the proteasome's substrate channel [2, 12]. Due to the
482 decline of proteasomal activity in various neurodegenerative diseases, elevated sPINK1
483 levels would consequently result in the cumulative increase of pUb. Thus, the elevation of
484 ubiquitin phosphorylation also constitutes a hallmark of neurodegeneration.

485 We further demonstrate that elevation of pUb level reciprocally contributes to UPS
486 dysfunction. Our findings reveal that increasing pUb levels through sPINK1* overexpression
487 exacerbated protein aggregation by impairing proteasomal degradation in both *in vitro* and *in*
488 *vivo* models. Conversely, *pink1* knockout reduces protein aggregation in aged mouse brains,
489 brains subjected to MCAO, and HEK293 cells treated with a proteasome inhibitor.
490 Mechanistically, we have found that ubiquitin phosphorylation negatively impacts both the
491 covalent elongation of ubiquitin chains, as previously reported [28], and the non-covalent
492 interaction between K48-linked polyUb chains and the proteasome, as discovered in the
493 current study, likely resulting from the increased ubiquitin structural dynamics upon
494 phosphorylation [26, 39]. This dual inhibitory mechanism hampers ubiquitination,
495 recruitment, and ultimately, degradation of substrate proteins by the proteasome. Impaired
496 proteasomal activity further impedes sPINK1 degradation, forming a self-amplifying cycle of

497 elevated pUb levels and progressive proteasomal dysfunction, culminating in the
498 accumulation of protein aggregates, the established hallmark of neurodegeneration.

499 Our findings indicate that elevated pUb levels can actively contribute to
500 neurodegeneration. Yet, the functional role of pUb appears nuanced: while transient pUb
501 elevation is generally neuroprotective, sustained elevation becomes neurotoxic. As a
502 neuroprotective mechanism, PINK1 activation upon mitochondrial damage leads to transient
503 phosphorylation of ubiquitin and Parkin, triggering mitophagy to remove damaged
504 mitochondria [30, 40, 41]. Indeed, PINK1 deficiency has been shown to cause
505 neurodegeneration, prompting the development of small-molecule activators [23, 40, 42].
506 However, in the current study, overexpression of a stable sPINK1 variant led to chronic
507 neuronal injury, resulting from the reciprocal relationship between proteasomal inhibition and
508 cumulative pUb elevation. The progressive decline in proteasomal function would
509 consequently disrupt cellular proteostasis and allow protein aggregates to build up. As such,
510 pUb is not simply a biomarker for neurodegeneration — sustained elevation is a driving
511 factor for progressive neuronal injury and neuroinflammation.

512 To confirm the neurotoxic effect of pUb, we utilized the phospho-null Ub/S65A mutant
513 to dilute pUb and antagonize its effects. Ub/S65A restored proteasomal activity *in vivo* and
514 even promoted the degradation of the stable sPINK1 variant, preventing its accumulation.
515 Moreover, Ub/S65A co-expression allowed the formation of longer polyUb chains, further
516 supporting its protective role. Conversely, overexpression of the phospho-mimetic Ub/S65E
517 mutant induced even more severe neuronal damage than sPINK1* overexpression. This effect
518 can be attributed to the 100% increase in mimicking pUb with Ub/S65E, whereas sPINK1*-
519 induced pUb levels are low and subjected to dephosphorylation [43, 44]. Similar toxic effects
520 resulting from Ub/S65E overexpression has been reported in yeast [29]. Furthermore, it

521 should be noted that, sPINK1* can phosphorylate both free and conjugated Ub, whereas
522 Ub/S65E only mimics monomeric pUb, potentially further contributing to the detrimental
523 effects of Ub/S65E mutant.

524 In conclusion, our findings have unveiled a novel pathogenetic mechanism of
525 neurodegeneration, in which the self-amplifying cycle of elevated pUb level and proteasomal
526 inhibition leads to the progressive decline of proteasomal activity and the accumulation of
527 toxic protein aggregates. Our findings demonstrate pUb is more than a consequence of this
528 gradual cumulative process, but also a critical contributor to disease progression. Targeting
529 this pUb-mediated self-amplifying cycle can be a viable therapeutic strategy to ameliorate the
530 progression of neurodegenerative diseases. On the other hand, elevated pUb levels observed
531 in a wide spectrum of neurodegenerative diseases may hinder the pharmacological efficacy of
532 drugs that target the UPS.

533

534 # Materials and Methods

535 **Human brain immunofluorescence staining**

536 The human brain cingulate gyrus paraffin section samples include two samples from
537 people with Alzheimer's Disease and two age-matched samples as the control. The samples
538 with AD were obtained from the Netherlands Brain Bank (NBB), Netherlands Institute for
539 Neuroscience, Amsterdam (Project number 1613), and the age matched control samples were
540 obtained from the National Health and Disease Human Brain Tissue Resource Center,
541 Hangzhou, China (Project number CN20240454). All material has been collected from
542 donors for or from whom a written informed consent for a brain autopsy and the use of the
543 material and clinical information for research purposes had been obtained by the NBB and
544 CBB. The detailed information of the donors is provided in Supplementary Table 1. The
545 experiments were conducted with approval from the Ethics Committee of the School of
546 Medicine, Zhejiang University, with the approval number ZJU2023-011.

547 For immunofluorescence staining, the samples was incubated at 62°C overnight to
548 dewax. The samples were then hydrated—Xylene for 3 times, 100% ethanol for 2 times, 95%
549 ethanol for 2 times, 75% ethanol for 2 times, and ddH_2O for 2 times. The samples were
550 placed in EDTA antigen retrieval solution, heated to 95-100°C for 30 minutes, and cooled
551 down at room temperature for 30 minutes. After washing with PBS buffer for 3 times, the
552 samples were placed in 3% H_2O_2 solution for 10 minutes. After washing with PBS buffer for
553 3 times, the samples were incubated in 0.3% Triton-X PBS for 30 minutes. After washing
554 with PBS buffer for 3 more times, the samples were permeabilized with 0.3% Tween in PBS
555 for 30 minutes, and rinsed 3 times with PBS to remove the detergent. The samples were
556 incubated in a solution with 5% Sudan black B (Aladdin Biochemical Technology Co., Ltd,
557 S109070-25g, Shanghai, China) and 70% ethanol for 1 min at room temperature.

558 Following PBS rinse, the samples were covered with the blocking solution (5% normal
559 goat serum, 2% bovine serum albumin, 0.1% Tween prepared in TBS-T) for 1 hr. The
560 samples were incubated with rabbit anti-PINK1 antibody (1:200, Novus, Colorado, USA,
561 BC100-494), rabbit anti-pUb antibody (1:200, Millipore, Massachusetts, USA, ABS1513), or
562 mouse anti-Aβ antibody (1:500, Biolegend, California, USA, SIG-39320) at 4 ºC overnight.
563 After washing with PBS for 3 times, the samples were incubated with Cy3-conjugated anti-
564 Rabbit IgG (1:200, Jackson, Pennsylvania, USA, 711-165-152) and fluorescein (FITC)-
565 conjugated anti-mouse IgG (1:200, Jackson, Pennsylvania, USA, 715-096-150) for 2 hrs at
566 room temperature. After washing with PBS for 3 times, the samples were mounted on the
567 slides using a ProLong™ Gold Antifade Mountant with DAPI (Invitrogen Corp., Carlsbad,
568 CA, USA). The immunofluorescence images were taken using an Olympus FV100 confocal
569 microscope.

570 **Animals**

571 The C57BL/6J and APP/PS1 mice were purchased from Zhejiang Academy of Medical
572 Science. All mice were kept in the Laboratory Animal Center, Zhejiang University School of
573 Medicine. The mice had free access to water and food in air-conditioned rooms (~26 °C,
574 relative humidity ~50%) on a 12-h light/dark cycle. Mice were handled following the Guide
575 for the Care and Use of the Laboratory Animals of the National Institutes of Health. The
576 experimental protocols were approved by the Ethics Committee of Laboratory Animal Care
577 and Welfare, Zhejiang University School of Medicine, with the approval number
578 ZJU20190138.

579 Using CRISPR-Cas9-mediated genome editing technology [45], the *pink1* gene
580 knockout mice (C57BL/6J) were customized purchased in Transgenic Mouse Laboratory of
581 Laboratory Animal Center of Zhejiang University. Briefly, two sgRNA sequences that target

582 exon 6 of the *pink1* gene were cloned into pX330-U6-Chimeric_BB-CBh-hSpCas9 plasmid
583 (a gift from Feng Zhang (Addgene plasmid # 42230; http://n2t.net/addgene: 42230; RRID:
584 Addgene 42230) using the *Bbsl* restriction site. The sequence of sgRNA1 is 5'-
585 GACAGCCATCTGCAGAGAGG-3', and the sequence of sgRNA2 is 5'-
586 GCAGGCAGGACTCACCTCAG-3'. The knockout of *pink1* gene was confirmed by using
587 DAN genotype, quantitative PCR, and Western blotting.

588 **Mouse hippocampus CA1 injection of Adeno-associated virus (AAV)**

589 The rAAV-EF1a-WPRE-hGH pA (AAV2/9) was used to specifically express proteins
590 within neurons, a bistronic vector expressing GFP and sPINK1* (PINK1/F101M/L102-L581)
591 as two separate proteins. Moreover, the rAAV-EF1a-Ub/S65A-P2A-sPINK1-P2A-EGFP-
592 WPRE-hGH pA can express GFP, sPINK1*, and Ub/S65A as three separate proteins, and
593 rAAV-EF1a-Ub/S65E-P2A-EGFP-WPRE-hGH pA can express GFP and Ub/S65E as two
594 separate proteins.

595 Mice of 9-months old were anesthetized with pentobarbital sodium (80 mg/kg) by
596 intraperitoneal injection (I.p.). Then the mice were fixed on a mouse stereotaxic holder (RWD
597 Life Science Co. LTP, China) for the injection of AAV. The distinct AAV was stereotactically
598 injected bilaterally into the CA1 region using a microinjector (Hamilton syringe) with a 31-
599 gauge needle and micropump (LEGATO 130 syringe pump, KD Scientific). After anesthesia
600 using pentobarbital sodium (100 mg/kg, i.p.), the injections were made at stereotaxic
601 coordinates of Bregma: anterioposterior (AP) = −1.7 mm, mediolateral (ML) =1.5 mm,
602 dorsoventral (DV) = 1.7 mm. A total 0.3 μl AAV (2.25×10^{12} viral particles/ml) was injected
603 into each side of the hippocampus.

604 **Behavioral tests**

605 Novel object recognition (NOR) was used to evaluate the spatial memory of mice
606 according to the previous report [46]. After handling for 5 days, the test was performed on the
607 68th day post injection. An open-field test system (ViewPoint Behavior Technology, France)
608 was used for NOR detection. During the training, two identical objects (named object A1 and
609 A2, 5 cm' 5 cm' 5 cm blue cone) was placed diagonally. The mouse was placed at the center
610 of the box, and the movement of the mouse was recorded for 10 min. After returning to the
611 home cage for 24 hrs, the mouse was put in the same box with one of the objects replaced by
612 a novel object in distinct color and shape (object B, 5 cm' 5 cm' 10 cm yellow cuboid). The
613 sniff number (number of visits) toward the objects was analyzed.

614 The fear conditioning test was performed in the Fear Conditioning System (Coulbourn
615 Instruments, USA) according to the previous report [46]. The freezing percentage was
616 recorded during each phase to analyze their memory. During the training phase, the mouse
617 was placed in the box (identified as box A) without any stimulation for 1.5 minutes. Then, a
618 tone (3000 Hz, 85 db) was applied for 30 seconds, and an electric shock (1 mA) was applied
619 at the final 2 seconds. After the shock, the mouse was kept in box A for 30 second, and was
620 put back to the home cage. The testing was performed at 24 hrs after training. The mouse was
621 placed back in the box A without any stimulation for 5 minutes, while the freezing percentage
622 in box A indicates contextual memory. Two hours after the test in box A, the mouse was
623 placed in a new box (identified to box B). For the first 2 minutes, no stimulus was given, and
624 subsequently, the same tone (3000 Hz, 85 db) was applied for the following 3 minutes. The
625 freezing percentage in box B without and with tone was used to analyze the cue memory of
626 the mice.

627 **Focal cerebral ischemia/reperfusion and Nissl staining**

628 After anesthetized, the mice were operated with middle cerebral artery occlusion
629 (MCAO) for 2 hrs ischemia followed by 24 hrs reperfusion. Briefly, a 6-0 nylon
630 monofilament suture was inserted into the internal carotid to occlude the origin of MCA [47].
631 Two hours after occlusion, the suture was withdrawn to allow reperfusion for 24 hrs. Mouse
632 body temperature was maintained at 37 °C using a thermostatic pad during and after surgery.
633 In sham-operated mice, the external carotid artery was surgically isolated but the suture was
634 no inserted.

635 For Nissl staining, the brain slices were incubated in a mixture of acetone and
636 chloroform (1:1) for 15 min, and then sequentially incubated in 100%, 95%, 70% alcohol for
637 5 min. Then the slices were stained for 10 min in Nissl staining containing 0.2% purple
638 crystal (Yuanhang Reagent Factory, Shanghai, China, YHSJ-01- 92) and 0.3% acetic acid.
639 Then, the slices were dehydrated by incubation in 70%, 95%, 100% alcohol. Finally, the
640 slices were put into xylene for 5 min and then mounted with a mixture of neutral resin and
641 xylene (1:1). The images were taken under a microscope (Olympus BX51, Japan).

642 **Mouse brain tissue collection**

643 Mice were anesthetized using pentobarbital sodium (150 mg/kg, i.p.). The mouse brains
644 were removed after transcardially perfused with 4 °C saline and freshly prepared 4%
645 paraformaldehyde. The brains were further fixed in 4% paraformaldehyde at 4 °C for one day
646 and transferred to 30% sucrose solution for dehydration. The brains were sliced into 30 μm
647 thick slices by cryomicrotomy (CM1900, Leica, Wetzlar, Germany). The slices were stored at
648 -20°C in the solution (30% glycerol, 30% glycol, 40% PBS) for immunofluorescence
649 staining, or stored in 2.5% glutaraldehyde for 12 hrs at 4 °C for transmission electron
650 microscopy (TEM) analysis.

651 For Western blotting, the mouse was transcardially perfused only with 4 °C saline. The
652 brains were removed, and the hippocampus was isolated. The hippocampus was quickly
653 frozen in liquid nitrogen and stored at -80 °C until use.

654 **Cell lines, cell culture, and cell transfection**

655 HEK293 cells and SH-SYT5Y cells were purchased from the Institute of Cell Biology
656 of the Chinese Academy of Sciences (Cell Biology of the Chinese Academy of Sciences,
657 Shanghai, China). The *pink1* gene knockout HEK293 cell was homely made using CRISPR-
658 Cas9-mediated genome editing technology[48]. PINK1 sgRNA
659 (CCTCATCGAGGAAAAACAGG) was cloned to U6-sgPINK1-mCherry plasmid (a gift
660 from John Doench & David Root (Addgene plasmid # 78038; http://n2t.net/addgene:78038 ;
661 RRID:Addgene_78038)). The U6-sgPINK1-mCherry plasmid and PX458-Cas9-EGFP
662 plasmid (a gift from Prof. Feng Zhang (Broad Institute, Cambridge, MA), Addgene plasmid
663 #48138) were co-transfected into HEK293 cells. The mCherry and GFP double-positive cells
664 were single-cell sorted 24 h post-transfection using an MoFloAstrios EQ cell sorter
665 (Beckman Coulter, US) and grown in separate cultures that were subsequently screened for
666 the presence of frameshift mutations leading to nonsense-mediated decay on both alleles.
667 PINK1 KO was confirmed using western blotting.

668 Cells were grown in Dulbecco's modified essential medium (DMEM, Gibco by Thermo
669 Fisher Scientific, C11995500BT) supplemented with 10% heat-inactivated fetal bovine serum
670 (FBS, Zhejiang Tianhang Biotechnology, China, 11011-8611) in the atmosphere of 5% CO_2
671 at 37 °C.

672 Lipo3000 (Invitrogen, California, USA, L3000001) was used to transfect plasmids,
673 following to the manufacturer' protocol. Briefly, an appropriate number of cells were seeded
674 one day before transfection with 70-80% confluent at the time of transfection. Before

675 transfection, plasmid DNA was carefully mixed with 250 μl Opti-MEM (Gibco by Life
676 Technologies, Carlsbad, USA). Subsequently, 250 μl Lipo3000 was carefully mixed with
677 Opti-MEM. The mixture was incubated at room temperature for 25 min. The freshly formed
678 DNA/Lipo3000 precipitates were carefully pipetted to the cells. The medium containing
679 transfection reagents was removed after 6 hrs and fresh medium was added.

680 At the end of treatments, the cells on cover slides were washed with 37 °C PBS and then
681 fixed using freshly prepared 4% paraformaldehyde. Subsequently, the cells were stored in
682 PBS under 4 °C for immunofluorescence staining.

683 **Oxygen glucose deprivation and reperfusion (OGD/R)**

684 Cells were washed twice by using glucose-free DMEM (Procell, PM150270) and
685 incubated at 37 °C with the ventilation of 95% N_2 and 5% CO_2 for 2 hours. The control cells
686 were washed twice by using high glucose DMEM, and incubated in 95% air and 5% CO_2
687 under 37 °C for 2 hours. Then the cells were cultured in the high glucose DMEM with 10%
688 FBS in 95% air and 5% CO_2 under 37 °C. This was identified as reperfusion.

689 **The construction of Ub-R-GFP vector**

690 The Ub-R-GFP is used for the *in vivo* measurement of proteasomal degradation activity, and
691 constructed according to a previous report[34]. Briefly, the ubiquitin open reading frame was
692 amplified by PCR with the following primers:

693 Sense primer: 5'-GCG GAATTCACCATGCAGATCTTCGTGAAGACT-3'
694 Antisense primer:
695 5'-GCG GGATCCTGTCGACCAAGCTTCCCGCGCCCACCTCTGAGACGGAGTAC-3'
696 The PCR product was cloned into the EcoRI and BamHI sites of the EGFP-N2 vector. Beside
697 the R residue, a 12 amino acid peptide was inserted between Ub and GFP to increase the

698 proteasomal degradation. Thus, the final product is Ub-R-GKLGRQDPPVAT-GFP. The
699 accumulation of GFP protein was used to determine the proteasomal degradation activity.

700 **Immunofluorescence staining**

701 The floating brain slices or cells on the cover glasses were incubated in 0.1% Triton-X
702 PBS for 30 min, and followed by the incubation in 5% donkey serum for 1 hr. The samples
703 were then incubated with mouse anti-ubiquitin antibody (1:200, Santa Cruz Biotechnology,
704 Texas, USA; SC-8017), rabbit anti-pUb antibody (1:200, Millipore, Massachusetts, USA;
705 ABS1513), rabbit anti-PINK1 antibody (1:200, Novus, Colorado, USA; BC100-494), mouse
706 anti-GFAP antibody (1:1000, CST, Pennsylvania, USA; #3670), rabbit anti-Iba1 antibody
707 (1:1000, FUJIFILM Wako Pure Chemical Corporation, Tokyo, Japan; 019-19741), rabbit
708 anti-NeuN antibody (1:1000, CST, Pennsylvania, USA; #36662), mouse anti-Aβ (1:500,
709 Biolegend, California, USA, SIG-39320) at 4 °C overnight. After washed with PBS (10 min'
710 3 times), the samples were incubated with Cy3 AffiniPure Donkey Anti-Mouse IgG (H+L)
711 (1:200, Jackson ImmunoResearch, PA, USA;715-605-150) or Cy3 AffiniPure Goat Anti-
712 Rabbit IgG (H+L) (1:200, Jackson ImmunoResearch, PA, USA;715-605-150; 111-165-003)
713 or Alexa Fluor488 AffiniPure Goat Anti-Rabbit IgG (H+L) (1:200,
714 Jackson ImmunoResearch, PA, USA; 111-545-003) or Alexa Fluor488 AffiniPure Goat Anti-
715 Rabbit IgG (H+L) (1:200, Jackson ImmunoResearch, PA, USA; 715-545-150) for 2 h. After
716 washing with PBS (10 min each for 3 times), the slices were mounted on slides using a
717 ProLong Gold Antifade Mountant with DAPI. The images were taken under an Olympus
718 FV100 confocal microscope (Olympus, Japan) and analyzed using MetaMorph (version
719 7.8.0.0, Molecular Devices, LLC. San Jose, CA 95134 USA).

720 **Western blot analysis**

721 The cells and brain tissues for the Western blot were lysed using RIPA lysis buffer
722 (Beyotime Biotechnology Research Institute, Jiangsu, China; P0013B) with protease inhibitor
723 (Beyotime Biotechnology Research Institute, Jiangsu, China; P1005) and phosphatase
724 inhibitor (Beyotime Biotechnology Research Institute, Jiangsu, China; P1081). The cells
725 were lysed on ice for 30 min, and every 10 min, the cells were gently vortexed. The brain
726 samples were thoroughly homogenized with a precooled TissuePrep instrument (TP-24,
727 Gering Instrument Company, Tianjin, China) for 1 min at 4 °C. Subsequently, the lysate was
728 centrifuged at 12,000 rpm for 30 min at 4 °C. The supernatant was first collected as the
729 soluble protein sample for Western blot analysis. The precipitate was resuspended in 20 μl
730 SDS buffer (2% SDS, 50 mM Tris-HCl, pH7.5) for ultrasonic pyrolysis at 4 °C. The
731 ultrasonic pyrolysis cycle included 10-sec ultrasonic pyrolysis (Diagenode, Seraing,
732 Belgium) and 30-sec interval, for a total of 8 cycles. The samples were then centrifuged at
733 12,000 rpm for 30 min at 4 °C. The supernatant was again collected as the insoluble protein
734 sample for Western blot analysis.

735 For brain tissues, the mice were anesthetized by intraperitoneal injection of
736 pentobarbital sodium (150 mg/kg) before sacrifice. The brains were quickly removed after
737 transcardially perfused with 4 °C saline. The hippocampus was separated and stored at -80 °C
738 until usage.

739 All protein concentration was determined by using BCA Protein Assay Kit (Beyotime
740 Biotechnology, Shanghai, China; P0009). Appropriate protein samples (50-100 μg) were used
741 for Western blot analysis. The following antibodies were used: mouse anti-Ub antibody
742 (1:800, Santa Cruz Biotechnology, Texas, USA; SC-8017), rabbit anti-pUb antibody (1:1000,
743 Millipore, Massachusetts, USA; ABS1513), rabbit anti-PINK1 antibody (1:1000, Novus,
744 Colorado, USA; BC100-494), mouse anti-GFAP antibody (1:1000, CST, Pennsylvania, USA;
745 #3670), rabbit anti-CD11b antibody (1:1000, Abcam, Cambridge, UK; ab133357), mouse

746 anti-GAPDH antibody (1:5000, Proteintech, Wuhan, China; 60004-1-Ig), mouse anti-MAP2
747 antibody (1:2000, Millipore, Billerica, MA, USA; AB5622), rabbit anti-PSD95 antibody
748 (1:1000, CST, Pennsylvania, USA; 3450S), rabbit anti-Tom20 antibody (1:1000,
749 Pennsylvania, USA; 42406S), rabbit anti-LC3 antibody (1:1000, Sigma, Massachusetts,
750 USA; L7543), rabbit anti-p62 antibody (1:1000, Abcam, California, USA; ab109012), mouse
751 anti-FLAG antibody (1:10000, TransGen biotech, Beijing, China; HT201-01). The secondary
752 antibody was HRP-conjugated goat anti-mouse IgG (1:3000, Cell Signaling Technology, MA,
753 USA; 7076S) or HRP-conjugated goat anti-rabbit IgG (1:10000, Jackson ImmunoResearch,
754 PA, USA, 111-035-003).

755 The immunoblots were then detected using ECL reagents (Potent ECL kit,
756 MultiSciences Biotech, Hangzhou, China; P1425) and measured using GBOX (LI-COR,
757 Odyssey-SA-GBOX, NE, USA). The results were normalized to GAPDH or Ponceau
758 staining (Beyotime Biotechnology Research Institute, Jiangsu, China; P0022), or to the
759 eGFP-expression control on the same immunoblot membrane.

760 **Golgi staining**

761 On the 70th-day post-transfection, mice were anesthetized by intraperitoneal injection of
762 pentobarbital sodium (150 mg/kg) before sacrifice. The mouse brain was quickly removed,
763 and the dorsal hippocampus was separated. The hippocampus was immediately fixed in the
764 fixative (Servicebio, Wuhan, China, G1101) for over 48 hrs.

765 The dorsal hippocampus was sliced with a thickness of 2-3 mm thickness around the
766 injection site. The tissue was gently rinsed with PBS at least 3 times. The hippocampus tissue
767 was then placed in Golgi-cox staining solution (Servicebio, Wuhan, China; G1069), and
768 incubated in a dark for 14 days. The Golgi-cox staining solution was changed 48 hrs after the
769 first soak, and every 3 days afterwards. On the14th-day after staining, the tissues were

770 immersed in distilled water for 3 times and then incubated in 80% acetic acid overnight until
771 the tissue became soft. After rinsing with distilled water, the tissue was placed into 30%
772 sucrose.

773 The tissue was cut into 100 μm slices with an oscillating microtome, and the slices were
774 placed on a gelatin slide and dried overnight in the dark. The sliced were then treated with
775 ammonia water for 15 min. After washing with distilled water, the slices were incubated in
776 the fixing solution for 15 min. After washing, the slices were sealed using glycerin gelatin.
777 Images were taken using VS120 Virtual Slide Microscope (Olympus, Japan).

778 **The *in vitro* ubiquitin-dependent proteasome degradation**

779 Ubiquitin was prepared as previously described [49, 50]. K48-linked di-ubiquitin and
780 tetra-ubiquitin were prepared following an established protocol [51], with the conjugation
781 reaction catalyzed by 2.5 μM human E1 and 20 μM E2-25K, in 20 mM pH 8.0 Tris-HCl
782 buffer. Ub/K48R mutant was incorporated as the distant Ub, and Ub/77D mutant was
783 incorporated as the proximal Ub to prepare Ub chain of the desired length. The residue D77
784 at the C-terminus was removed with hydrolase YUH1. The fusion protein His-TEV-Ub-GFP
785 was prepared recombinantly based on the design previously described [34, 52]. The
786 *Pediculus humanus corporis* PINK1 kinase (phPINK1) was prepared and purified as
787 previously described [26, 27]. Ub phosphorylation was confirmed with electrospray mass
788 spectrometry (Agilent G6530 Q-TOF).

789 The 26S proteasome from HEK293 cells was prepared following an established
790 protocol, with the purification tag appended at the C-terminus of Rpn11 [53, 54]. The
791 proteasome activity was assessed with a fluorogenic peptide, N-succinyl-Leu-Leu-Val-Tyr-7-
792 amido-4-methyl coumarin (Sigma, Massachusetts, USA; S6510). A final concentration of 100
793 nM proteasome and 100 μM proteasome peptide substrate was prepared in the reaction

794 buffer, containing 50 mM Tris-HCl pH 7.5, 4 mM ATP (Sigma- Aldrich, Cat# A6559) and 5
795 mM $MgCl_2$. The fluorescence intensity of the product was measured by a fluorometer
796 (Horiba Scientific, FluoroMax-4) at an excitation wavelength of 360 nm.

797 For Western blot analysis of GFP, 200 nM proteasomal substrate and 10 nM human 26S
798 proteasome were prepared in 20 mM Tris pH 8.0 buffer, with 50 mM NaCl, 5 mM ATP, and 5
799 mM $MgCl_2$. The mixture was incubated at 37 ° C for 0, 10, 30, 60, 90, and 120 min. At each
800 time point, 20 μL samples were taken for Western blot analysis. A mouse anti-GFP antibody
801 (1:2000, San-Ying Proteintech Group, 66002-1) and an HRP-conjugated goat anti-mouse IgG
802 (1:3000, CST, Pennsylvania, USA; 7076S) were used. ImageJ was used to analyze the band
803 intensities, which are normalized to the initial intensity.

804 The recombinant Ub, pUb (phosphorylated by phPINK1), Ub/S65A, and Ub/S65E were
805 reacted with 2.5 μM human E1 and 20 μM E2-25K in 20 mM pH 8.0 Tris-HCl buffer. The
806 formed Ub chain was determined by Coomassie blue staining on SDS page gel.

807 **TIRF analysis of ubiquitin-proteasome interaction**

808 The coverslips were prepared following an established protocol [55]. Each coverslip
809 was divided into multiple lanes with double-sided tape for parallel TIRF experiments, thus to
810 ensure repeatability with different proteins added to the same slide. Streptavidin (VWR Life
811 Science, Cat# 97062-808) in imaging buffer at a concentration of 50 μg/ml was loaded;
812 excess unbound streptavidin was washed away. The imaging buffer contains 25 mM Tris-HCl
813 (pH 7.5), 50 mM NaCl, 10 mM MgCl2, 40 mM imidazole, 5 m/mL BSA (Sigma-Aldrich),
814 2.5 mM ADP (Sigma-Aldrich), and 0.5 mM ATP-γ-S (Sigma-Aldrich), as previously
815 described [35].

816 The purified human 26S proteasome at 20 nM in the imaging buffer was added to the
817 streptavidin-immobilized coverslip, with excess unbound proteins washed away with the

818 imaging buffer. The substrate protein, either K48-polyUb-GFP or pK48-polyUb-GFP, was
819 then added to the coverslip to a final concentration of 400 pM. The imaging was performed
820 on a Nikon A1 TIRF microscope equipped with a 488 nm laser and an EMCCD camera
821 (Andor DU-897). The time series were acquired at 300 ms per frame for a total duration of 2
822 min for each time series. The view area was 512 pixels by 512 pixels (16 by 16 μm), and the
823 experiments were repeated four times on four different proteasome-immobilized cover slides.
824 The puncta density was counted in iSMS software [56] with default settings. Only when the
825 substrate protein becomes bound to the immobilized proteasome, the green puncta can be
826 observed, and only the puncta with brightness above a certain threshold (≥ 3000 a.u.) and the
827 dwell time of more than three consecutive frames are selected for counting the overall
828 number of puncta. The dwell times were tabulated in 300 ms bins and fitted with single
829 exponential decay.

830 **Proteomics analysis**

831 Hippocampus samples were rinsed using PBS and lysed in RIPA lysis buffer. The
832 samples were then denatured at 95 °C for 5 min, followed by sonication at 4 °C (3 s on, 3 s
833 off, with 30% amplitude). The lysate was centrifuged at 16,000 g for 10 min at 4 °C, and the
834 supernatant was collected as whole tissue extract. Protein concentration was determined by
835 Bradford protein assay. Extracts from the protein sample (2 g) were trypsin digested.
836 The enriched peptides sample were precipitated in solution A (0.1% formic acid), and
837 was centrifuged at 16,000 g for 10 min. The peptides were separated on a reverse-phase
838 nano-HPLC C18 column (Precolumn, 3 μm, 120 Å, 2x100 i.d.; analysis column, 1.9 μm 120
839 Å, 30 cm x150 μm, i.d.) at a flow rate of 600 nL/min with a 150 min gradient of 7-95%
840 solution B (0.1% formic acid in acetonitrile). For peptide ionization, 2100 V was applied, and
841 a 320 ºC capillary temperature was used. For detection with Q Exactive HF, peptides were

842 analyzed with one full scan (350–1400 m/z, R = 120,000 at 200 m/z) with an automatic gain
843 control target of $3x10^6$ ions, with max injection time of 80 ms, followed by up to 30 data-
844 dependent MS/MS scans with high-energy collision dissociation (target 5 $x10^4$ ions, max
845 injection time 19 ms, isolation window 1.6 m/z, normalized collision energy of 27%),
846 detected in the Orbitrap (R = 15,000 at 200 m/z). Dynamic exclusion time was set as 30 sec.

847 Raw MS data were searched against the mouse National Center for Biotechnology
848 Information (NCBI) Refseq protein database (updated on 2013/07/01, 29764 entries) by the
849 software Thermo Proteome Discoverer 2.1 using Mascot 2.3. The mass tolerances were 20
850 ppm for precursor and 50 mmu for product ions for Q Exactive HF. The search engine set
851 Acetyl(Protein N-term), oxidation(M), Phospho(ST), Phospho(Y) as variable modifications.
852 Trypsin digestion of up to two missed cleavages was allowed. The peptide identifications
853 were accepted at a false discovery rate (FDR) of 1%. Using a label-free approach, a unique
854 peptide was used to represent the absolute abundance of a particular peptide across the
855 sample.

856 For the proteomic data analysis, quantile normalization was applied to eliminate batch
857 effect, and missing values were imputed using the minimum value observed in the dataset.
858 The differentially expressed proteins were defined with the following these criteria: an
859 increase by more than two-fold or decrease by more than 50%. For Gene Set Enrichment
860 Analysis (GSEA) analysis, Gene Ontology (GO) analysis was conducted by GSEApy
861 (version 0.10.5) Python package to evaluate the enriched GO terms. The association of
862 proteins with GO terms was derived from the DAVID database. For Gene Set Enrichment
863 Analysis (GSEA), the ranking metric used was the fold change, and significantly enriched
864 GO terms were filtered with a cutoff *P*-value of 0.05.

865 **Statistical analysis**

Data are presented as mean ±SD. GraphPad Prism Software (version 6.0, GraphPad Software, San Diego, CA, USA) was used for statistical analysis and plot graphs. The ROUT test was used to identify outliers. The Brown-Forsythe test was used to evaluate the equal variances of the data. D'Agonstino-Pearson omnibus normality test was performed to test the normality of the data. If the data pass the normality test and equal variance test, *t*-test, the parametric one-way ANOVA (Tukey multiple comparisons test), or two-way ANOVA (Newman-Keuls multiple comparisons test) was used. If not, nonparametric test (Dunn's multiple comparisons test) was used. Chi-square test was also used to assess the differences in categorical data distributions. $P<0.05$ was considered statistically significant.

Author contributions

W.P.Z. and C.T. designed the study and wrote the manuscript. C.C., T.Y.G., H.W.Y., Y.Z., T.Y., T.W., and T.F.W. conducted the experiments. Y.B.L. and W.P.Z. analyzed the data at mouse and cellular level. T.T.L. analyzed the proteomic data. C.T. analyzed the data at protein level.

Acknowledgements

This study was supported by the National Key R&D Program of China (2023YFF1200007) to C.T. and W.P.Z., and (2021YFF1200900) to T.T.L., the National Natural Science Foundation of China (92353304) to C.T. and (32070666) to T.T.L..

Data availability

All data needed to evaluate the conclusions in the paper are present in the paper and/or the Supplementary Materials.

References

1. Wilson, D.M., 3rd, et al., *Hallmarks of neurodegenerative diseases.* Cell, 2023. **186**(4): p. 693-714.
2. McDade, E., et al., *Ubiquitin-Proteasome System in the Different Stages of Dominantly Inherited Alzheimer's Disease.* Res Sq, 2024.
3. Kinger, S., et al., *Proteostasis in neurodegenerative diseases.* Adv Clin Chem, 2024. **121**: p. 270-333.
4. Davidson, K. and A.M. Pickering, *The proteasome: A key modulator of nervous system function, brain aging, and neurodegenerative disease.* Front Cell Dev Biol, 2023. **11**: p. 1124907.
5. Krishna, K.K., T. Behnisch, and S. Sajikumar, *Modulation of the Ubiquitin-Proteasome System Restores Plasticity in Hippocampal Pyramidal Neurons of the APP/PS1 Alzheimer's Disease-Like Mice.* J Alzheimers Dis, 2022. **86**(4): p. 1611-1616.
6. Costa, R.O., et al., *Synaptogenesis Stimulates a Proteasome-Mediated Ribosome Reduction in Axons.* Cell Rep, 2019. **28**(4): p. 864-876 e6.
7. Soykan, T., V. Haucke, and M. Kuijpers, *Mechanism of synaptic protein turnover and its regulation by neuronal activity.* Curr Opin Neurobiol, 2021. **69**: p. 76-83.
8. Swatek, K.N. and D. Komander, *Ubiquitin modifications.* Cell Res, 2016. **26**(4): p. 399-422.
9. Komander, D. and M. Rape, *The ubiquitin code.* Annu Rev Biochem, 2012. **81**: p. 203-29.
10. Pohl, C. and I. Dikic, *Cellular quality control by the ubiquitin-proteasome system and autophagy.* Science, 2019. **366**(6467): p. 818-822.
11. Wojcik, C. and M. Di Napoli, *Ubiquitin-proteasome system and proteasome inhibition: new strategies in stroke therapy.* Stroke, 2004. **35**(6): p. 1506-18.
12. Tseng, B.P., et al., *Abeta inhibits the proteasome and enhances amyloid and tau accumulation.* Neurobiol Aging, 2008. **29**(11): p. 1607-18.
13. Herhaus, L. and I. Dikic, *Expanding the ubiquitin code through post-translational modification.* EMBO Rep, 2015. **16**(9): p. 1071-83.
14. Koyano, F., et al., *Ubiquitin is phosphorylated by PINK1 to activate parkin.* Nature, 2014. **510**(7503): p. 162-6.
15. Hou, X., et al., *Age- and disease-dependent increase of the mitophagy marker phospho-ubiquitin in normal aging and Lewy body disease.* Autophagy, 2018. **14**(8): p. 1404-1418.
16. Fiesel, F.C., et al., *(Patho-)physiological relevance of PINK1-dependent ubiquitin phosphorylation.* EMBO Rep, 2015. **16**(9): p. 1114-30.
17. Shiba-Fukushima, K., et al., *Evidence that phosphorylated ubiquitin signaling is involved in the etiology of Parkinson's disease.* Hum Mol Genet, 2017. **26**(16): p. 3172-3185.
18. Okatsu, K., et al., *Unconventional PINK1 localization to the outer membrane of depolarized mitochondria drives Parkin recruitment.* J Cell Sci, 2015. **128**(5): p. 964-78.
19. Okatsu, K., et al., *A dimeric PINK1-containing complex on depolarized mitochondria stimulates Parkin recruitment.* J Biol Chem, 2013. **288**(51): p. 36372-84.
20. Yamano, K. and R.J. Youle, *PINK1 is degraded through the N-end rule pathway.* Autophagy, 2013. **9**(11): p. 1758-69.

938 21. Takatori, S., G. Ito, and T. Iwatsubo, *Cytoplasmic localization and proteasomal*
939 *degradation of N-terminally cleaved form of PINK1.* Neurosci Lett, 2008. **430**(1): p.
940 13-7.
941 22. Lazarou, M., et al., *The ubiquitin kinase PINK1 recruits autophagy receptors to induce*
942 *mitophagy.* Nature, 2015. **524**(7565): p. 309-314.
943 23. Chin, R.M., et al., *Pharmacological PINK1 activation ameliorates Pathology in*
944 *Parkinson's Disease models.* bioRxiv, 2023.
945 24. Gao, J., et al., *Cytosolic PINK1 promotes the targeting of ubiquitinated proteins to the*
946 *aggresome-autophagy pathway during proteasomal stress.* Autophagy, 2016. **12**(4):
947 p. 632-47.
948 25. Tang, C. and W.P. Zhang, *How Phosphorylation by PINK1 Remodels the Ubiquitin*
949 *System: A Perspective from Structure and Dynamics.* Biochemistry, 2020. **59**(1): p. 26-
950 33.
951 26. Dong, X., et al., *Ubiquitin S65 phosphorylation engenders a pH-sensitive*
952 *conformational switch.* Proc Natl Acad Sci U S A, 2017. **114**(26): p. 6770-6775.
953 27. Wauer, T., et al., *Mechanism of phospho-ubiquitin-induced PARKIN activation.* Nature,
954 2015. **524**(7565): p. 370-4.
955 28. Wauer, T., et al., *Ubiquitin Ser65 phosphorylation affects ubiquitin structure, chain*
956 *assembly and hydrolysis.* EMBO J, 2015. **34**(3): p. 307-25.
957 29. Swaney, D.L., R.A. Rodriguez-Mias, and J. Villen, *Phosphorylation of ubiquitin at Ser65*
958 *affects its polymerization, targets, and proteome-wide turnover.* EMBO Rep, 2015.
959 **16**(9): p. 1131-44.
960 30. Shiba-Fukushima, K., et al., *Phosphorylation of mitochondrial polyubiquitin by PINK1*
961 *promotes Parkin mitochondrial tethering.* PLoS Genet, 2014. **10**(12): p. e1004861.
962 31. Gan, Z.Y., et al., *Activation mechanism of PINK1.* Nature, 2022. **602**(7896): p. 328-335.
963 32. Beilina, A., et al., *Mutations in PTEN-induced putative kinase 1 associated with*
964 *recessive parkinsonism have differential effects on protein stability.* Proc Natl Acad Sci
965 U S A, 2005. **102**(16): p. 5703-8.
966 33. Samant, R.S., et al., *Distinct proteostasis circuits cooperate in nuclear and*
967 *cytoplasmic protein quality control.* Nature, 2018. **563**(7731): p. 407-411.
968 34. Dantuma, N.P., et al., *Short-lived green fluorescent proteins for quantifying*
969 *ubiquitin/proteasome-dependent proteolysis in living cells.* Nat Biotechnol, 2000.
970 **18**(5): p. 538-43.
971 35. Lu, Y., et al., *Substrate degradation by the proteasome: a single-molecule kinetic*
972 *analysis.* Science, 2015. **348**(6231): p. 1250834.
973 36. Hegde, A.N., et al., *The Proteasome and Ageing.* Subcell Biochem, 2023. **102**: p. 99-
974 112.
975 37. Lambourne, O.A., et al., *PINK1-Dependent Mitophagy Inhibits Elevated Ubiquitin*
976 *Phosphorylation Caused by Mitochondrial Damage.* J Med Chem, 2023. **66**(11): p.
977 7645-7656.
978 38. Chen, C., et al., *The Role of Ubiquitin-Proteasome Pathway and Autophagy-Lysosome*
979 *Pathway in Cerebral Ischemia.* Oxid Med Cell Longev, 2020. **2020**: p. 5457049.
980 39. Qin, L.Y., et al., *Kinetic Constraints in the Specific Interaction between Phosphorylated*
981 *Ubiquitin and Proteasomal Shuttle Factors.* Biomolecules, 2021. **11**(7).
982 40. Li, J., et al., *PINK1/Parkin-mediated mitophagy in neurodegenerative diseases.* Ageing
983 Res Rev, 2023. **84**: p. 101817.

41. Agarwal, S. and M.M.K. Muqit, *PTEN-induced kinase 1 (PINK1) and Parkin: Unlocking a mitochondrial quality control pathway linked to Parkinson's disease.* Curr Opin Neurobiol, 2022. **72**: p. 111-119.
42. Hertz, N., et al., *Pharmacological PINK1 activation ameliorates Pathology in Parkinson's Disease models.* Res Sq, 2024.
43. Wall, C.E., et al., *PPEF2 Opposes PINK1-Mediated Mitochondrial Quality Control by Dephosphorylating Ubiquitin.* Cell Rep, 2019. **29**(10): p. 3280-3292 e7.
44. Wang, L., et al., *PTEN-L is a novel protein phosphatase for ubiquitin dephosphorylation to inhibit PINK1-Parkin-mediated mitophagy.* Cell Res, 2018. **28**(8): p. 787-802.
45. Cong, L., et al., *Multiplex genome engineering using CRISPR/Cas systems.* Science, 2013. **339**(6121): p. 819-23.
46. Shen, C., et al., *The Depletion of NAMPT Disturbs Mitochondrial Homeostasis and Causes Neuronal Degeneration in Mouse Hippocampus.* Mol Neurobiol, 2023. **60**(3): p. 1267-1280.
47. Shi, W.Z., et al., *Aggravated chronic brain injury after focal cerebral ischemia in aquaporin-4-deficient mice.* Neurosci Lett, 2012. **520**(1): p. 121-5.
48. Ran, F.A., et al., *Genome engineering using the CRISPR-Cas9 system.* Nat Protoc, 2013. **8**(11): p. 2281-2308.
49. Liu, Z., et al., *Lys63-linked ubiquitin chain adopts multiple conformational states for specific target recognition.* Elife, 2015. **4**: p. e05767.
50. Liu, Z., et al., *Noncovalent dimerization of ubiquitin.* Angewandte Chemie. International Ed. In English, 2012. **51**(2): p. 469-72.
51. Pickart, C.M. and S. Raasi, *Controlled synthesis of polyubiquitin chains.* Methods Enzymol, 2005. **399**: p. 21-36.
52. Inobe, T., et al., *Defining the geometry of the two-component proteasome degron.* Nat Chem Biol, 2011. **7**(3): p. 161-7.
53. Huang, X., et al., *An atomic structure of the human 26S proteasome.* Nat Struct Mol Biol, 2016. **23**(9): p. 778-85.
54. Guerrero, C., et al., *An integrated mass spectrometry-based proteomic approach: quantitative analysis of tandem affinity-purified in vivo cross-linked protein complexes (QTAX) to decipher the 26 S proteasome-interacting network.* Mol Cell Proteomics, 2006. **5**(2): p. 366-78.
55. Roy, R., S. Hohng, and T. Ha, *A practical guide to single-molecule FRET.* Nat Methods, 2008. **5**(6): p. 507-16.
56. Preus, S., et al., *iSMS: single-molecule FRET microscopy software.* Nat Methods, 2015. **12**(7): p. 593-4.